Analysis of Planar and Curved Microstrip Antennas

Ralf T. Jacobs, Arnulf Kost,
Brandenburg University of Technology, Cottbus, Germany
jacobs/kost@aet.tu-cottbus.de
Hajime Igarashi,
Hokkaido University, Sapporo, Japan
Alan J. Sangster
Heriot-Watt University, Edinburgh, UK

***Abstract*— A finite element-boundary integral method has been developed to investigate the impedance and radiation characteristics of planar and conformal cavity backed microstrip patch antennas. In case of conformal antennas, the radiating element is mounted on a cylindrical surface. The effect of curvature is analysed and the impact of the cavity size on the performance of the radiating element is investigated. For the examples considered, it is shown that the simulated results are in good agreement with measurement.**

Index Terms— Finite element-boundary integral method, impedance and radiation characteristics, microstrip patch antenna

I. INTRODUCTION

Microstrip patch antennas are employed as radiating or receiving elements in a wide range of microwave systems such as radar, navigation, communication, remote sensing and biomedical systems. The radiating elements in these applications are usually considered to be planar but more recent developments seek to mould antennas into curved surfaces. Particular examples for this are radar antennas integrated into the body of an aircraft, mm-wave imaging arrays mounted on unmanned airborne vehicles (UAVs), and antennas for medical imaging applications which may be required to conform to the shape of the human body. In many potential developments the surface may also be subject to flexing as a result of mechanical forces acting on the structure, and the radiating elements need to be tolerant to this. Cavity-backed patch elements in stripline have been found to be particularly suitable to this type of application. A finite element-boundary integral (FE-BI) procedure is employed for the investigation. The hybrid method has the advantage to reduce the discretization requirements for the finite element formulation to a minimum without affecting its modelling flexibility. The boundary integral provides an exact mesh termination condition on the aperture surface of the antenna and circumvents the need to introduce artificial boundary conditions based on, for example, absorbing boundary conditions [1], [2] or perfectly matched layer techniques [3], [4]. Hybrid FE-BI procedures have been applied to solve a variety of radiation and scattering problems in two- and three-dimensions [5], [6]. Patch antennas with arbitrary shaped patch elements and planar patches in array environments have been considered

Brazilian Microwave and Optoelectronics Society-SBMO Received 10 Aug., 2006; revised 2 Feb., 2007; accepted 14 May, 2007
ISSN 1516-7399

in [7]–[9], where the radar cross section formed the focal point of the investigation. Scattering by cavity-backed antennas on a circular cylinder has been investigated in [10]. Asymptotic expressions for the dyadic Green's functions of a cylinder were employed in [10], and these enabled an efficient evaluation of the boundary integrals which significantly reduced the required computation time for the boundary integral subsystem. Patch antennas on ferromagnetic substrates have been analysed in [11], where the substrate region was discretized using brick elements and anisotropic material characteristics were considered. A hybrid formulation for scattering from anisotropic test objects using tetrahedral elements is outlined in [12]. The boundary integral formulation leads to a densely populated matrix since the interactions between all degrees of freedom on the boundary need to be computed. The assemblage of the matrix as well as the system solution are computationally extensive and time consuming. An efficient solution can be achieved if a uniform discretization of the boundary surface is applied which enables to recast the boundary integral matrix into a Toeplitz matrix. This then allows the implementation of an iterative solver where the evaluation of the matrix-vector product is performed in the spectral domain. The technique has been used in several of the papers cited above and a short description of the computational advantages of the method will be given in section III. Section II of the paper provides a brief derivation of finite element-boundary integral procedure used for the antenna analysis. Summaries as well as historical reviews of the FE-BI method are given in [13], [14], whereas detailed derivations of various aspects of finite element and boundary element methods can be found in [15]–[18]. The novelty of this implementation rests on a fast evaluation of the boundary integrals using a coordinate transformation which reduces the number of integrations required to compute the interactions between the degrees of freedom on the aperture surface of the antenna. The purpose of the investigation is the analysis of the radiation and impedance characteristics of patch elements embedded in planar and cylindrically curved surfaces. The impact of curvature on the performance of a patch antenna is analysed, the influence of the cavity size is investigated, and the effect of tolerances of the dielectric substrate material is examined. The accuracy of the numerical method is verified through measurements.

II. Method of Analysis

The geometries of the planar and curved antenna structures under consideration are depicted in Fig. 1. The patch of length l_i^{p} is backed by a cavity of length l_i^{c}, where the subscript i represents the appropriate direction in Cartesian (x, y, z) or cylindrical (ρ, φ, z) coordinates. $\mathcal{S}$ symbolises the aperture surface. The patch element is excited using a coaxial probe feed positioned at l_i^{F}. The height of the cavity domain $\mathcal{D}$ is determined by the thickness of the dielectric substrate which is characterised by the relative permittivity ε_r and the loss tangent $\tan\delta$. The relative permeability μ_r of the substrate equals unity. The computation of the impedance properties and the radiation characteristics of the

Brazilian Microwave and Optoelectronics Society-SBMO Received 10 Aug., 2006; revised 2 Feb., 2007; accepted 14 May, 2007
ISSN 1516-7399

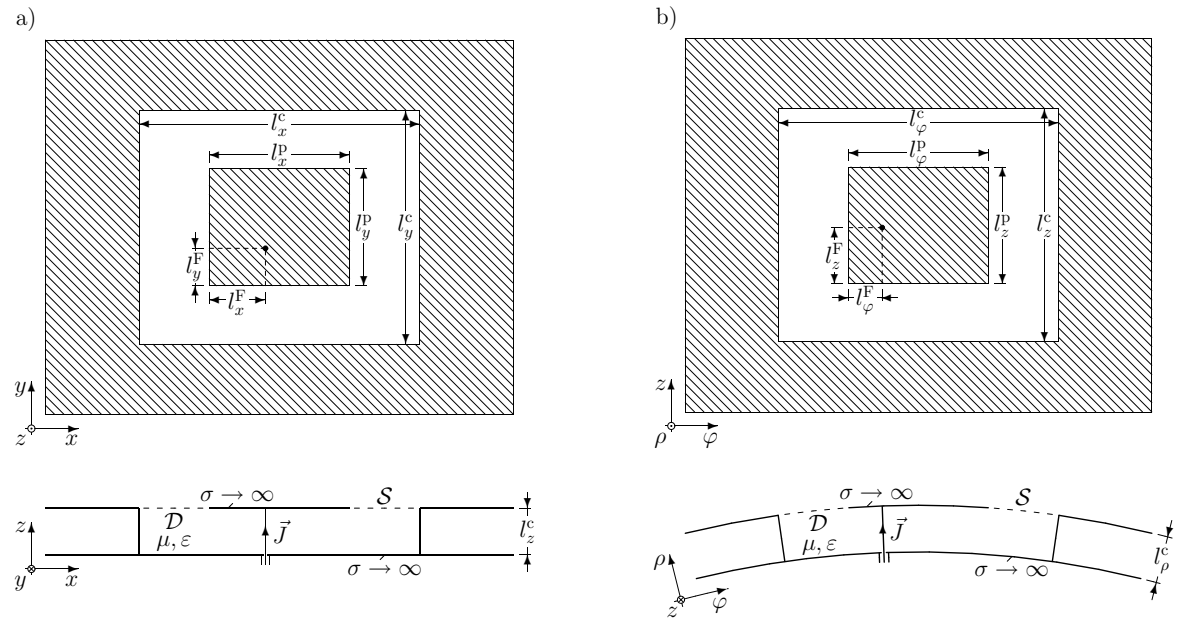

Fig. 1. Antenna dimensions: a) planar structure, b) curved structure.

antenna is performed employing a finite element-boundary integral method [7], [14], [18]–[20]. The electric field $\vec{E}$ in the cavity domain satisfies the wave equation

$$\nabla \times \frac{1}{\mu_r} \nabla \times \vec{E} - k_0^2 \varepsilon_r \vec{E} + j k_0 Z_0 \sigma \vec{E} = -j k_0 Z_0 \vec{J}, \tag{1}$$

subject to the boundary condition

$$\vec{n} \times \vec{E} = 0 \tag{2}$$

on conducting cavity walls. k_0 symbolises the wavenumber and Z_0 the characteristic impedance of free space. $\vec{J}$ denotes the electric current density, and σ the conductivity of the medium. The vector wave equation of the electric field is converted into weak form applying the weighted residual method [15], [21]. Multiplying both sides of (1) with a set of weighting functions $\vec{v}_i, i = 1 \ldots N$, and integrating over the cavity volume $\mathcal{D}$ leads to

$$\iiint_{\mathcal{D}} \left[\nabla \times \frac{1}{\mu_r} \nabla \times \vec{E} - k_0^2 \varepsilon_r \vec{E} + j k_0 Z_0 \sigma \vec{E} \right] \cdot \vec{v}_i \, dV = -j k_0 Z_0 \iiint_{\mathcal{D}} \vec{J} \cdot \vec{v}_i \, dV \,, \quad \forall i \in [1, N] \,. \tag{3}$$

Application of Green's first integral theorem [22] results in

$$\begin{aligned} \iiint_{\mathcal{D}} \left[\frac{1}{\mu_r} \left(\nabla \times \vec{E} \right) \cdot \left(\nabla \times \vec{v}_i \right) - k_0^2 \varepsilon_r \vec{E} \cdot \vec{v}_i + j k_0 Z_0 \sigma \vec{E} \cdot \vec{v}_i \right] dV \\ - \oiint_{\partial \mathcal{D}} \frac{1}{\mu_r} \left[\vec{v}_i \times \nabla \times \vec{E} \right] \cdot \vec{n} \, dS = -j k_0 Z_0 \iiint_{\mathcal{D}} \vec{J} \cdot \vec{v}_i \, dV \,, \qquad \forall i \in [1, N] \,, \end{aligned} \tag{4}$$

Brazilian Microwave and Optoelectronics Society-SBMO Received 10 Aug., 2006; revised 2 Feb., 2007; accepted 14 May, 2007
ISSN 1516-7399

and subsequent employment of Maxwell's second equation to the curl of the electric field in the contour integral yields the weak form of the wave equation,

$$\begin{aligned}\iiint_{\mathcal{D}} \left[\frac{1}{\mu_r}\left(\nabla\times\vec{E}\,\right)\cdot\left(\nabla\times\vec{v}_i\right) - k_0^2\varepsilon_r\vec{E}\cdot\vec{v}_i + jk_0Z_0\sigma\vec{E}\cdot\vec{v}_i\right]dV \\ - jk_0Z_0\oiint_{\partial\mathcal{D}}\left[\vec{n}\times\vec{H}\right]\cdot\vec{v}_i\,dS = -jk_0Z_0\iiint_{\mathcal{D}}\vec{J}\cdot\vec{v}_i\,dV\,, \qquad \forall i\in[1,N]\,.\end{aligned} \tag{5}$$

The contour integral reduces to a double integral over the aperture surface $\mathcal{S}$ as a result of the Dirichlet condition on the cavity walls. The tangential magnetic field $\vec{H}$ on the aperture surface equals the radiated magnetic field $\vec{H}^{\text{rad}}$ since no sources are located outside the cavity volume. $\vec{H}^{\text{rad}}$ is determined by the tangential electric field on the aperture and the appropriate dyadic Green's function $\vec{\vec{G}}(\vec{r},\vec{r}\,')$ for the outer half-space [23], [24],

$$\vec{H}^{\text{rad}}(\vec{r}) = -jk_0Y_0\iint_{\mathcal{S}'}\vec{\vec{G}}(\vec{r},\vec{r}\,')\cdot(\vec{n}\times\vec{E}(\vec{r}\,'))\,dS'\,, \tag{6}$$

where $\vec{r}$ denotes the field vector, $\vec{r}\,'$ the source vector, $\vec{n}$ the outward pointing normal vector, and $Y_0 = 1/Z_0$ the characteristic admittance of free space. Explicit expressions for the dyadic Green's functions are given in the appendix. The coaxial probe feed is modelled as current filament since the size of the probe element is only a very small fraction of the operating wavelength. The current density in the probe is described by

$$\vec{J}_z = I_0\,\delta(x-x_F)\,\delta(y-y_F)\,\vec{e}_z, \qquad \text{for planar,} \tag{7}$$

$$\vec{J}_\rho = I_0\,(\delta(\varphi-\varphi_F)/\rho)\,\delta(z-z_F)\,\vec{e}_\rho, \qquad \text{for cylindrical} \tag{8}$$

structures, where the angle φ_F of the feed position is determined through the arc length l_φ^{F} and the radius ρ of the cylinder. I_0 denotes the current in the feed element and $\vec{e}_i$ the unit vector in i-direction. Applying the Galerkin procedure and expanding the electric field in (5) with the same set of functions as the weighting functions

$$\vec{E} = \sum_{j=1}^{N} a_j\vec{v}_j\,, \tag{9}$$

yields a set of linear equations which can be solved for the coefficients a_j. The resulting system of equations can be written as

$$(\mathbf{P}+\mathbf{Q})\cdot\mathbf{a} = \mathbf{b}\,, \tag{10}$$

where the column vector $\mathbf{a} = [a_1, a_2, \ldots, a_N]^T$ contains the coefficients to be determined. The vector $\mathbf{b}$ symbolises the excitation vector, of which the entries are defined by

$$b_i = -jk_0Z_0\iiint_{\mathcal{D}}\vec{J}\cdot\vec{v}_i\,dV\,, \qquad \forall i\in[1,N]\,. \tag{11}$$

Brazilian Microwave and Optoelectronics Society-SBMO Received 10 Aug., 2006; revised 2 Feb., 2007; accepted 14 May, 2007
ISSN 1516-7399

$\mathbf{P}$ represents the resulting finite element matrix

$$P_{ij} = \iiint\limits_{\mathcal{D}} \left[\frac{1}{\mu_r} (\nabla \times \vec{v}_j) \cdot (\nabla \times \vec{v}_i) - k_0^2 \varepsilon_r \, \vec{v}_j \cdot \vec{v}_i + j k_0 Z_0 \sigma \, \vec{v}_j \cdot \vec{v}_i \right] dV \,, \qquad \forall i,j \in [1,N] \,, \quad (12)$$

and $\mathbf{Q}$ the boundary integral matrix

$$Q_{ij} = k_0^2 \iint\limits_{\mathcal{S}} (\vec{n} \times \vec{v}_i) \cdot \iint\limits_{\mathcal{S}'} \vec{\vec{G}}(\vec{r}, \vec{r}\,') \cdot (\vec{n} \times \vec{v}_j) \, dS' dS \,, \qquad \forall i,j \in [1, N^S] \,. \quad (13)$$

N^S denotes the number of degrees of freedom on the aperture surface. The cavity domain is discretized with curl-conforming edge elements which match the coordinate system of the underlying problem domain. This technique eliminates geometrical approximation errors. In the planar case rectangular parallelepipeds are used and for the conformal case the cavity is discretized with cylindrical shell elements, where in both cases a uniform discretization of the aperture surface is applied. The elements naturally fit in the problem structure and allow an exact discretization of the geometry. Linear interpolation functions are defined on the elements and the mesh is terminated on the aperture surface with the aid of the boundary integral formulation. The elements and interpolation functions are described in [15], [16]. An analytical solution of the boundary integrals is not attainable due to the Green's function in the integral kernel, but the application of a coordinate transformation allows the reduction of the four-fold integration to a sum of four double integrations which enables a numerically efficient evaluation of the boundary integral formulation. The finite element matrix $\mathbf{P}$ is sparse, whereas the boundary integral formulation leads to a densely populated matrix $\mathbf{Q}$ since the interactions between all degrees of freedom on the aperture surface need to be computed. The required computation time to assemble a dense subsystem is prohibitively large and the storage requirements would restrict the applicability of the hybrid procedure to small scale problems. These limitations can be lifted by exploiting the properties of the uniform discretization of the aperture surface, which enables the circumvention of the explicit computation of the full boundary integral matrix. The technique to achieve this will be outlined together with the coordinate transformation of the boundary integrals in section III. The matrix equation (10) is solved using the biconjugate gradient method [25], [26], which determines the expansion coefficients a_j. The input impedance Z_{in} of the patch element is computed employing the reaction concept [27],

$$\begin{aligned} Z_{\text{in}} &= -\frac{1}{I_0^2} \iiint\limits_{\mathcal{D}} \vec{E} \cdot \vec{J} \, dV \,, \\ &= -\frac{1}{I_0^2} \sum_{j=1}^{N} a_j \iiint\limits_{\mathcal{D}} \vec{v}_j \cdot \vec{J} \, dV \,, \end{aligned} \quad (14)$$

Brazilian Microwave and Optoelectronics Society-SBMO Received 10 Aug., 2006; revised 2 Feb., 2007; accepted 14 May, 2007
ISSN 1516-7399

and the radiation characteristics are evaluated using equation (6) in conjunction with the electric field expansion in (9),

$$\vec{H}^{\text{rad}} = -jk_0Y_0 \sum_{j=1}^{N^{\text{S}}} a_j \iint\limits_{\mathcal{S}} \vec{\vec{G}}(\vec{r},\vec{r}\,') \cdot (\vec{n} \times \vec{v}_j)\, dS' \,. \tag{15}$$

The far-field relations

$$E_\theta = Z_0 H_\varphi \,, \tag{16}$$

$$E_\varphi = -Z_0 H_\theta \,, \tag{17}$$

determine the radiated electric field, where the angles θ and φ denote the spherical coordinates.

III. Boundary Integral Evaluation

The contribution Q_{ij} of the boundary integral formulation to the system equation is determined by the four-fold integral in (13), where the weighting and expansion functions, $\vec{v}_i$ and $\vec{v}_j$, are defined using linear interpolation functions. A fragment of the discretized aperture surface with surface coordinates ξ

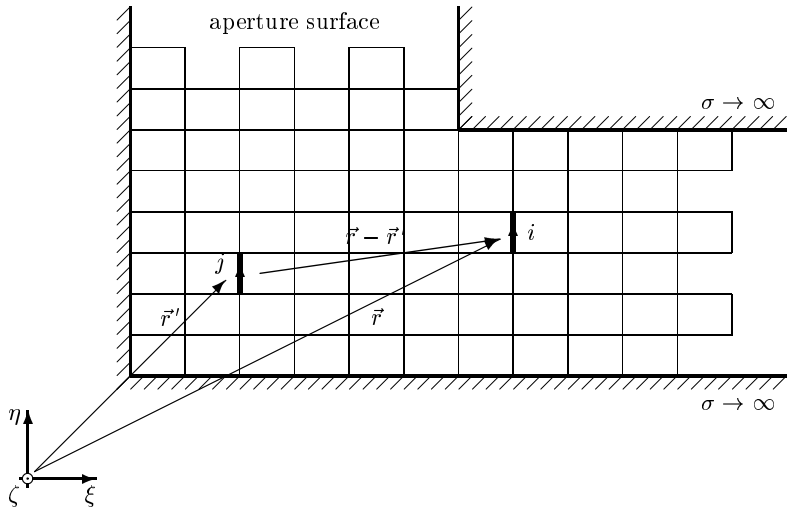

Fig. 2. Fragment of the discretized aperture surface

and η is depicted in Fig. 2. The surface elements are described by

$$\begin{aligned} S &= \left\{ (\xi,\eta) \in \mathbb{R}^2 \,\middle|\, \xi_0 \le \xi \le \xi_1, \eta_0 \le \eta \le \eta_1 \right\}, \\ S' &= \left\{ (\xi',\eta') \in \mathbb{R}^2 \,\middle|\, \xi'_0 \le \xi' \le \xi'_1, \eta'_0 \le \eta' \le \eta'_1 \right\}. \end{aligned} \tag{18}$$

The evaluation of the quadruple integral in (13) is extremely time consuming since all interactions between source and field edges on the aperture need to be computed. The integral kernel possesses a convolutional property which can be exploited to recast the boundary integral subsystem into a block Toeplitz matrix if a uniform discretization of the aperture surface is applied. This enables the reduction of the storage requirements since a Toeplitz matrix of size $N \times N$ can be stored as vector of length $2N - 1$. The block Toeplitz structure also enables the implementation of a fast iterative

Brazilian Microwave and Optoelectronics Society-SBMO Received 10 Aug., 2006; revised 2 Feb., 2007; accepted 14 May, 2007
ISSN 1516-7399

solver where the matrix-vector product involving the boundary integral subsystem is performed in the spectral domain employing Fast Fourier Transforms [28]–[30]. Detailed descriptions of FFT-based matrix-vector products in conjunction with conjugate gradient solvers are outlined in [31]. A technique to further reduce the required computation time for the boundary integrals rests on the application of a coordinate transformation. Although (13) cannot be solved analytically, the four-fold integration can be reduced to a sum of four double integrations. The matrix entries for both planar and cylindrical elements have the form

$$Q_{ij} = k_0^2 \int_{\eta_0}^{\eta_1} \int_{\xi_0}^{\xi_1} f_i(\xi,\eta) \int_{\eta_0'}^{\eta_1'} \int_{\xi_0'}^{\xi_1'} G(\xi,\eta,\xi',\eta') \cdot f_j(\xi',\eta')\, d\xi' d\eta'\, d\xi\, d\eta\,, \tag{19}$$

where $G(\xi,\eta,\xi',\eta')$ symbolizes the appropriate element of the dyadic Green's function, and $f_i(\xi,\eta)$ and $f_j(\xi',\eta')$ the scalar components of the relevant shape functions. The Green's functions are only dependent upon the difference $\vec{r}-\vec{r}\,'$ between the field and source vectors as illustrated in Fig. 2. This property can be used to reduce the quadruple integral to double integrals by introducing the coordinate transformation:

$$\begin{aligned} \xi &= \frac{\nu+\kappa}{2}\,, & \eta &= \frac{\chi+\varsigma}{2}\,, \\ \xi' &= \frac{\nu-\kappa}{2}\,, & \eta' &= \frac{\chi-\varsigma}{2}\,. \end{aligned} \tag{20}$$

The domains of integration are depicted in Fig. 3. The boundaries of κ and ς in the transformed

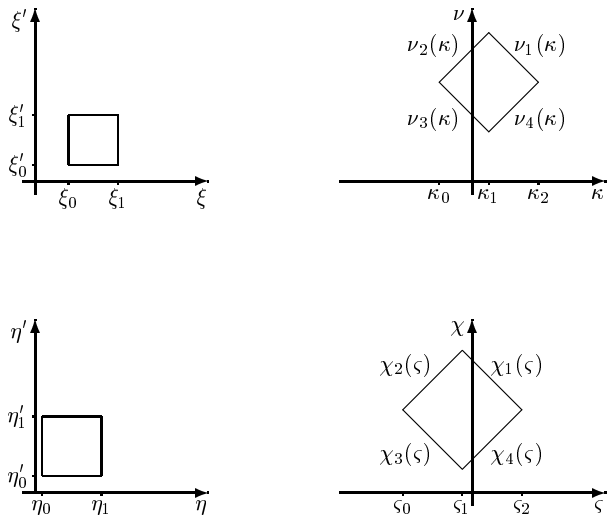

Fig. 3. Domains of integration

domain are given by $\kappa = \left[\xi_0 - \xi_1', \xi_1 - \xi_0'\right]$ and $\varsigma = \left[\eta_0 - \eta_1', \eta_1 - \eta_0'\right]$, whereas the boundaries of the integrals over ν and χ are dependent upon κ and ς. The Jacobian determinants evaluate as

$$\frac{\partial(\xi,\xi')}{\partial(\kappa,\nu)} = \frac{1}{2} \qquad \text{and} \qquad \frac{\partial(\eta,\eta')}{\partial(\varsigma,\chi)} = \frac{1}{2}\,. \tag{21}$$

Brazilian Microwave and Optoelectronics Society-SBMO Received 10 Aug., 2006; revised 2 Feb., 2007; accepted 14 May, 2007
ISSN 1516-7399

The Green's functions $G(\xi,\eta,\xi',\eta')$ are only dependent upon κ and ς in the transformed domain. Applying the change of variables to (19) leads to

$$Q_{ij} = \frac{k_0^2}{4}\Bigg[\int_{\varsigma_0}^{\varsigma_1}\int_{\kappa_0}^{\kappa_1} G(\kappa,\varsigma)\,\Upsilon_{ij}^{\mathrm{I}}(\kappa,\varsigma)\,d\kappa\,d\varsigma + \int_{\varsigma_0}^{\varsigma_1}\int_{\kappa_1}^{\kappa_2} G(\kappa,\varsigma)\,\Upsilon_{ij}^{\mathrm{II}}(\kappa,\varsigma)\,d\kappa\,d\varsigma + \int_{\varsigma_1}^{\varsigma_2}\int_{\kappa_0}^{\kappa_1} G(\kappa,\varsigma)\,\Upsilon_{ij}^{\mathrm{III}}(\kappa,\varsigma)\,d\kappa\,d\varsigma + \int_{\varsigma_1}^{\varsigma_2}\int_{\kappa_1}^{\kappa_2} G(\kappa,\varsigma)\,\Upsilon_{ij}^{\mathrm{IV}}(\kappa,\varsigma)\,d\kappa\,d\varsigma\Bigg], \tag{22}$$

where the functions $\Upsilon_{ij}^{k}(\kappa,\varsigma)$, are defined as

$$\begin{aligned}
\Upsilon_{ij}^{\mathrm{I}}(\kappa,\varsigma) &= \int_{\chi_3(\varsigma)}^{\chi_2(\varsigma)}\int_{\nu_3(\kappa)}^{\nu_2(\kappa)} f_i(\kappa,\nu,\varsigma,\chi)\,f_j(\kappa,\nu,\varsigma,\chi)\,d\nu\,d\chi\,,\\
\Upsilon_{ij}^{\mathrm{II}}(\kappa,\varsigma) &= \int_{\chi_3(\varsigma)}^{\chi_2(\varsigma)}\int_{\nu_4(\kappa)}^{\nu_1(\kappa)} f_i(\kappa,\nu,\varsigma,\chi)\,f_j(\kappa,\nu,\varsigma,\chi)\,d\nu\,d\chi\,,\\
\Upsilon_{ij}^{\mathrm{III}}(\kappa,\varsigma) &= \int_{\chi_4(\varsigma)}^{\chi_1(\varsigma)}\int_{\nu_3(\kappa)}^{\nu_2(\kappa)} f_i(\kappa,\nu,\varsigma,\chi)\,f_j(\kappa,\nu,\varsigma,\chi)\,d\nu\,d\chi\,,\\
\Upsilon_{ij}^{\mathrm{IV}}(\kappa,\varsigma) &= \int_{\chi_4(\varsigma)}^{\chi_1(\varsigma)}\int_{\nu_4(\kappa)}^{\nu_1(\kappa)} f_i(\kappa,\nu,\varsigma,\chi)\,f_j(\kappa,\nu,\varsigma,\chi)\,d\nu\,d\chi\,.
\end{aligned} \tag{23}$$

These functions represent integrals over linear interpolation polynomials which can be solved analytically. The solutions can be written as polynomials of third degree with constant coefficients $a_0,\ldots,a_3$ and $b_0,\ldots,b_3$ which take the form

$$\Upsilon_{ij}^{k}(\kappa,\varsigma) = \left(a_{3_{kij}}\kappa^3 + a_{2_{kij}}\kappa^2 + a_{1_{kij}}\kappa + a_{0_{kij}}\right)\cdot\left(b_{3_{kij}}\varsigma^3 + b_{2_{kij}}\varsigma^2 + b_{1_{kij}}\varsigma + b_{0_{kij}}\right). \tag{24}$$

The analytical solutions of the integrals in (23) reduce the boundary integral in (22) to a sum of four double integrals which are then evaluated numerically. The coordinate transformation significantly reduces the required computation for the boundary integral formulation since the quadruple integration is circumvented.

IV. Simulated Results

In order to initially validate the numerical procedure a planar patch element of size $l_x^{\mathrm{p}} = 90\,\mathrm{mm}$ and $l_y^{\mathrm{p}} = 60\,\mathrm{mm}$ is analysed for two different feed positions. Fig. 4 shows the impedance loci which display good agreement with measurement and reflect the known tendency of the radiation resistance to increase as the feed element approaches the edge of the patch. The excitation of the patch antenna is accomplished employing a coaxial probe feed which is modelled as current filament. The simplified model of the feed, which does not account for the finite probe diameter, is susceptible to cause inaccuracies but the validity of the model is supported by the fact that measured impedances for

Brazilian Microwave and Optoelectronics Society-SBMO Received 10 Aug., 2006; revised 2 Feb., 2007; accepted 14 May, 2007
ISSN 1516-7399

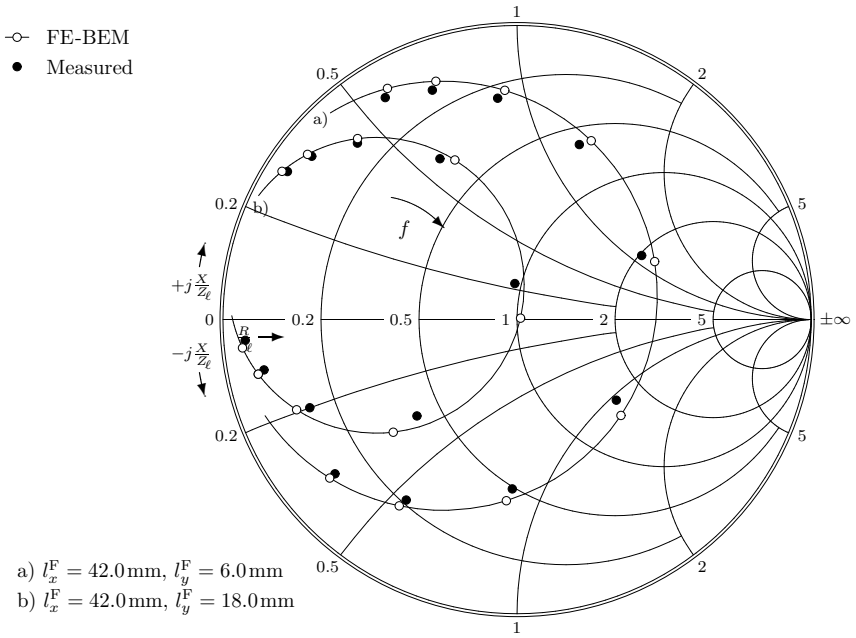

Fig. 4. Input impedance of a planar patch antenna for different feed positions, $f = 1.60\,\mathrm{GHz} \ldots 1.68\,\mathrm{GHz}$, $\Delta f = 0.01\,\mathrm{GHz}$, $l_x^{\mathrm{p}} = 90\,\mathrm{mm}$, $l_y^{\mathrm{p}} = 60\,\mathrm{mm}$, $l_x^{\mathrm{c}} = 135\,\mathrm{mm}$, $l_y^{\mathrm{c}} = 90\,\mathrm{mm}$, $l_z^{\mathrm{c}} = 0.762\,\mathrm{mm}$, $\varepsilon_r = 2.20$, $\tan\delta = 0.0008$, $Z_\ell = 50\,\Omega$

different probe diameters show no significant variation of the impedance characteristics. Fig. 5 displays

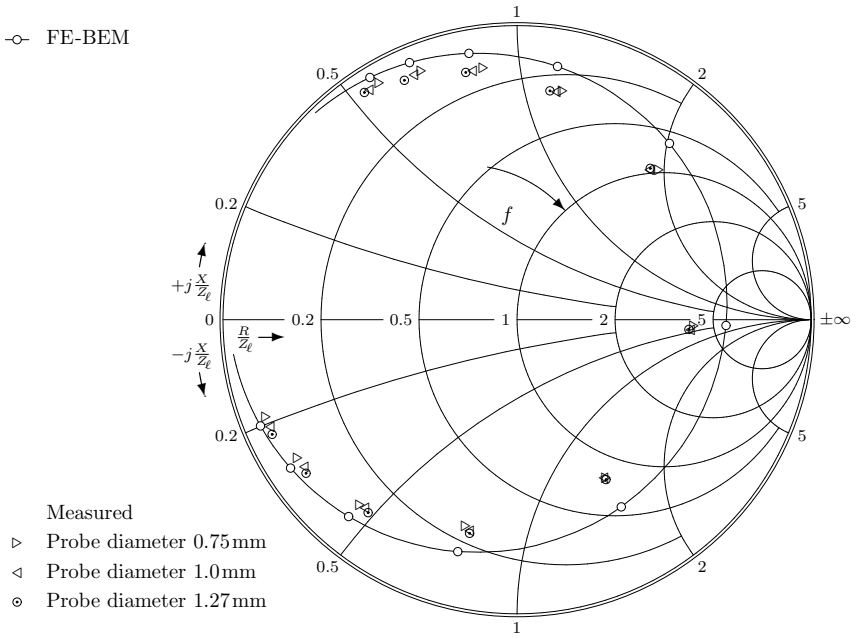

Fig. 5. Input impedance of a planar patch antenna with different probe diameters, $f = 2.10\,\mathrm{GHz} \ldots 2.30\,\mathrm{GHz}$, $\Delta f = 0.02\,\mathrm{GHz}$, $l_x^{\mathrm{p}} = 45\,\mathrm{mm}$, $l_y^{\mathrm{p}} = 30\,\mathrm{mm}$, $l_x^{\mathrm{c}} = 60\,\mathrm{mm}$, $l_y^{\mathrm{c}} = 40\,\mathrm{mm}$, $l_z^{\mathrm{c}} = 0.762\,\mathrm{mm}$, $l_x^{\mathrm{F}} = 11.25\,\mathrm{mm}$, $l_y^{\mathrm{F}} = 7.5\,\mathrm{mm}$, $\varepsilon_r = 2.20$, $\tan\delta = 0.0008$, $Z_\ell = 50\,\Omega$

computed and measured results for a patch antenna of size $l_x^{\mathrm{p}} = 45\,\mathrm{mm}$ and $l_y^{\mathrm{p}} = 30\,\mathrm{mm}$, fed by coaxial probes of diameters $0.75\,\mathrm{mm}$, $1.0\,\mathrm{mm}$ and $1.27\,\mathrm{mm}$. The marginal differences between the measured impedances cannot necessarily be attributed to the different probe diameters, since these could also have been induced through measurement inaccuracies or fabrication tolerances.

Brazilian Microwave and Optoelectronics Society-SBMO Received 10 Aug., 2006; revised 2 Feb., 2007; accepted 14 May, 2007
ISSN 1516-7399

To investigate the effect of the cavity dimensions on the input impedance of a planar microstrip antenna, a square patch element of dimension $l_x^{\mathrm{p}} = 35\,\mathrm{mm}$ and $l_y^{\mathrm{p}} = 35\,\mathrm{mm}$ is analysed. The substrate material of the antenna has a thickness of $l_z^{\mathrm{c}} = 0.762\,\mathrm{mm}$, a relative permittivity of $\varepsilon_r = 2.20$, and a loss tangent of 0.0008. Simulations and measurements are performed for cavity sizes $l_{x,y}^{\mathrm{c}}$ equal to 1.25, 1.5 and 2.0 times the patch size. The results are also compared to measured impedance properties of a patch antenna without cavity, which is centred on a substrate of eight times the size of the patch. The Smith chart in Fig. 6 shows good agreement between theory and measurement. Only marginal differences between the input impedance values for the cavity backed and unbacked

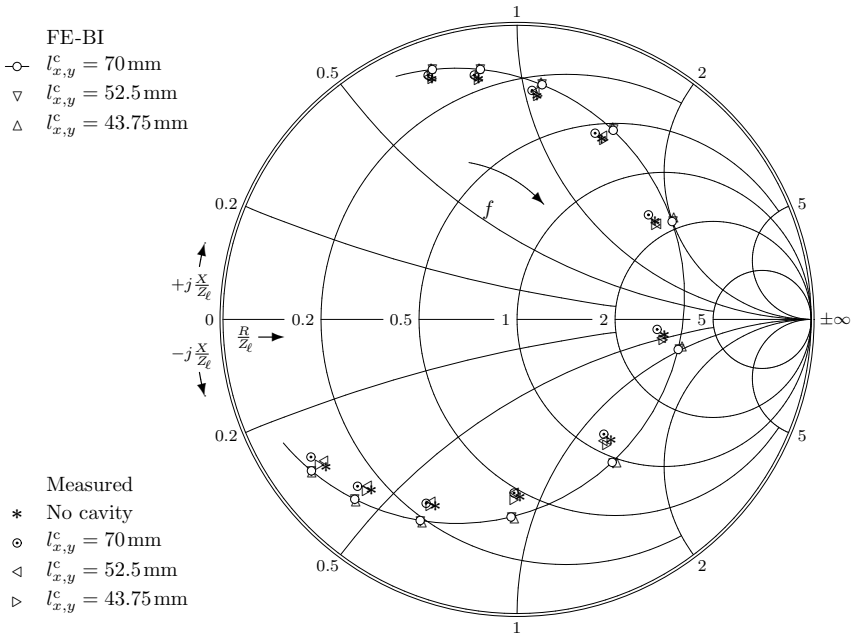

Fig. 6. Input impedance of a planar patch antenna for different cavity sizes, $f = 2.70\,\mathrm{GHz} \ldots 2.90\,\mathrm{GHz}$, $\Delta f = 0.02\,\mathrm{GHz}$, $l_x^{\mathrm{p}} = 35\,\mathrm{mm}$, $l_y^{\mathrm{p}} = 35\,\mathrm{mm}$, $l_z^{\mathrm{c}} = 0.762\,\mathrm{mm}$, $l_x^{\mathrm{F}} = 17.5\,\mathrm{mm}$, $l_y^{\mathrm{F}} = 7.5\,\mathrm{mm}$, $\varepsilon_r = 2.20$, $\tan\delta = 0.0008$, $Z_\ell = 50\,\Omega$.

patch antennas are observable, which indicates that the chosen cavity dimensions have very little effect on the impedance properties of a patch antenna. Fig. 7 shows the E-plane radiation pattern for a circumferentially polarized patch antenna, and Fig. 8 the H-plane radiation pattern of an axially polarized patch antenna for different cavity sizes. The patch elements are mounted on a cylinder of radius $\rho = 149.5\,\mathrm{mm}$. The finite element-boundary integral computations show good agreement with measurement and cavity model results from [32]. Only minor deviations are observable between the radiation patterns for the different cavity sizes, which confirms that the chosen cavity sizes have very little effect on the antenna performance. This behaviour can be ascribed to the fact that radiation occurs from the edge fields only, which are in the close proximity to the perimeter of the patch. If the cavity walls are sufficiently distant from the patch, such that the fringing fields on the edge are not perturbed, the radiation characteristics of the antenna remain unaltered. The effect of curvature on the input impedance is investigated by computing the characteristics of a patch element for different

Brazilian Microwave and Optoelectronics Society-SBMO Received 10 Aug., 2006; revised 2 Feb., 2007; accepted 14 May, 2007
ISSN 1516-7399

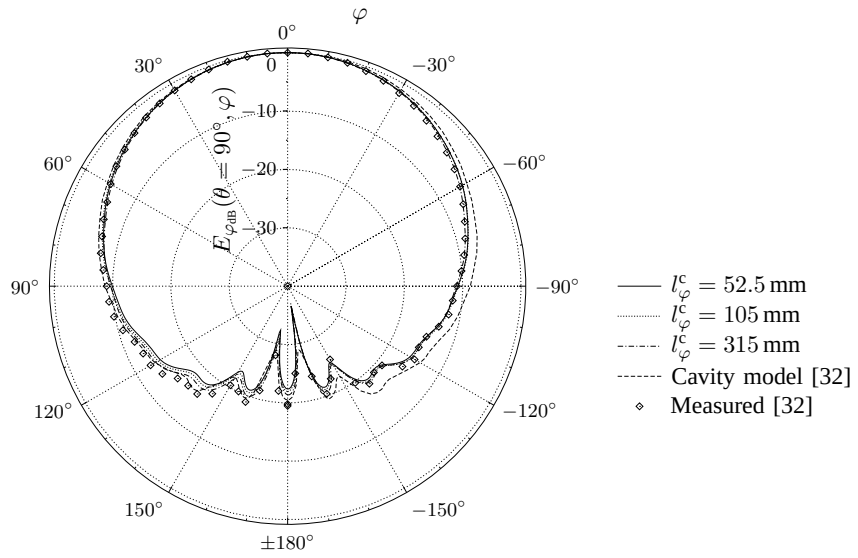

Fig. 7. E-plane radiation pattern of a circumferentially polarized patch antenna for different cavity sizes, $l_\varphi^{\mathrm{p}} = 35\,\mathrm{mm}$, $l_z^{\mathrm{p}} = 35\,\mathrm{mm}$, $l_z^{\mathrm{c}} = 70\,\mathrm{mm}$, $l_\rho^{\mathrm{c}} = 3.175\,\mathrm{mm}$, $\rho = 149.5\,\mathrm{mm}$, $l_\varphi^{\mathrm{F}} = 30\,\mathrm{mm}$, $l_z^{\mathrm{F}} = 17.5\,\mathrm{mm}$, $\varepsilon_r = 2.32$, $\tan\delta = 0.00015$, $f = 2.615\,\mathrm{GHz}$

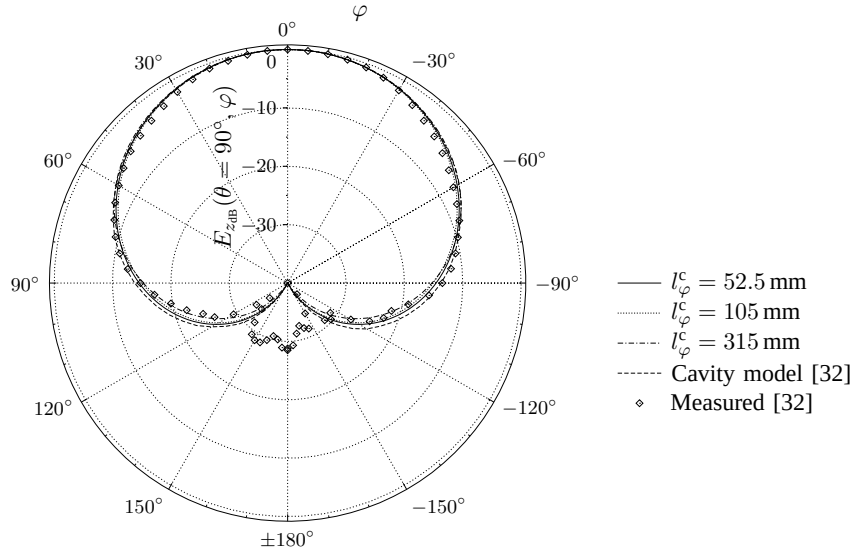

Fig. 8. H-plane radiation pattern of an axially polarized patch antenna for different cavity sizes, $l_\varphi^{\mathrm{p}} = 35\,\mathrm{mm}$, $l_z^{\mathrm{p}} = 35\,\mathrm{mm}$, $l_z^{\mathrm{c}} = 70\,\mathrm{mm}$, $l_\rho^{\mathrm{c}} = 3.175\,\mathrm{mm}$, $\rho = 149.5\,\mathrm{mm}$, $l_\varphi^{\mathrm{F}} = 17.5\,\mathrm{mm}$, $l_z^{\mathrm{F}} = 5.0\,\mathrm{mm}$, $\varepsilon_r = 2.32$, $\tan\delta = 0.00015$, $f = 2.615\,\mathrm{GHz}$

cylinder radii. Cylinders of radii ρ of $122.5\,\mathrm{mm}$, $175\,\mathrm{mm}$ and $350\,\mathrm{mm}$ are considered, and results are compared to the properties of an equivalent planar antenna. The Smith chart in Fig. 9 displays the input impedance of an axially polarized patch antenna. The simulations show only minor differences between the loci for the different radii. Fig. 10 depicts the impedance properties of a circumferentially polarized patch antenna. The Smith chart also exhibits only slight variations between the characteristics for the different curvatures. The computed impedances for both polarizations tend as expected towards the locus of the equivalent planar case for an increasing cylinder radius. The differences between the impedance values in the limited range of practically realizable radii of curvature are of the same order

Brazilian Microwave and Optoelectronics Society-SBMO Received 10 Aug., 2006; revised 2 Feb., 2007; accepted 14 May, 2007
ISSN 1516-7399

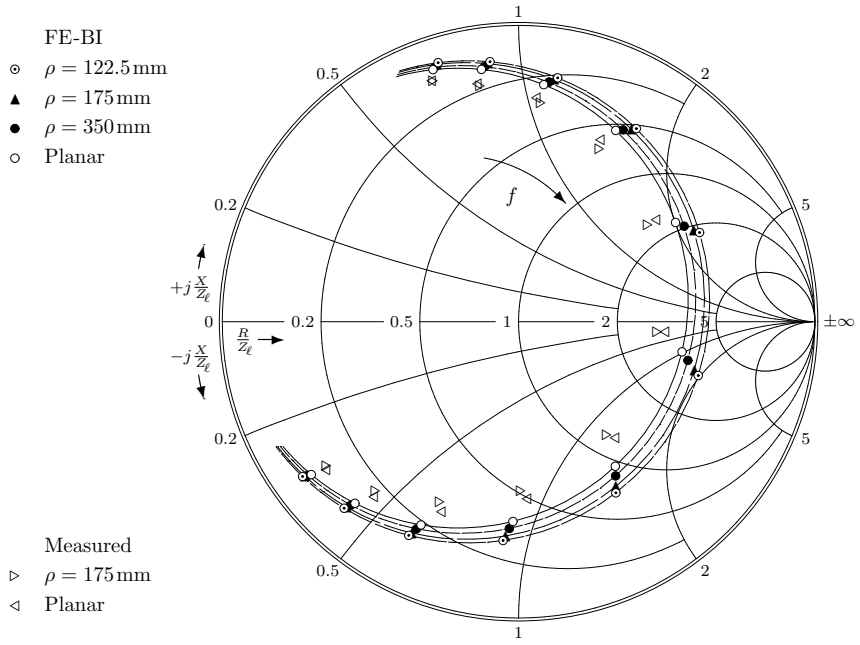

Fig. 9. Input impedance of an axially polarized patch antenna for different cylinder radii, $f = 2.70\,\mathrm{GHz} \ldots 2.90\,\mathrm{GHz}$, $\Delta f = 0.02\,\mathrm{GHz}$, $l_\varphi^\mathrm{p} = 35\,\mathrm{mm}$, $l_z^\mathrm{p} = 35\,\mathrm{mm}$, $l_\rho^\mathrm{c} = 0.762\,\mathrm{mm}$, $l_\varphi^\mathrm{c} = 52.5\,\mathrm{mm}$, $l_z^\mathrm{c} = 52.5\,\mathrm{mm}$, $l_\varphi^\mathrm{F} = 17.5\,\mathrm{mm}$, $l_z^\mathrm{F} = 7.5\,\mathrm{mm}$, $\varepsilon_r = 2.20$, $\tan\delta = 0.0008$, $Z_\ell = 50\,\Omega$.

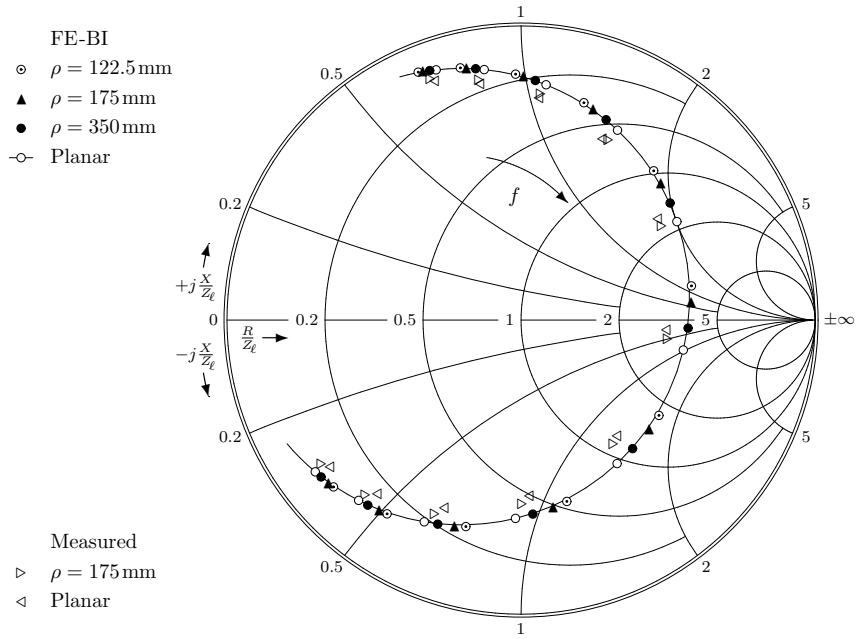

Fig. 10. Input impedance of a circumferentially polarized patch antenna for different cylinder radii, $f = 2.70\,\mathrm{GHz} \ldots 2.90\,\mathrm{GHz}$, $\Delta f = 0.02\,\mathrm{GHz}$, $l_\varphi^\mathrm{p} = 35\,\mathrm{mm}$, $l_z^\mathrm{p} = 35\,\mathrm{mm}$, $l_\rho^\mathrm{c} = 0.762\,\mathrm{mm}$, $l_\varphi^\mathrm{c} = 52.5\,\mathrm{mm}$, $l_z^\mathrm{c} = 52.5\,\mathrm{mm}$, $l_\varphi^\mathrm{F} = 27.5\,\mathrm{mm}$, $l_z^\mathrm{F} = 17.5\,\mathrm{mm}$, $\varepsilon_r = 2.20$, $\tan\delta = 0.0008$, $Z_\ell = 50\,\Omega$.

of magnitude as measurement inaccuracies and fabrication tolerances. The stresses on the substrate, induced by the forces exerted to attain conformality, potentially affect its permittivity and possibly provoke a slight non-linear geometrical deformation of the structure. These effects combine, and affect the accuracy of the measured impedance characteristics of conformal patch antennas. Despite these small unpredictable effects, the simulations and measurements suggest that no significant mismatch

Brazilian Microwave and Optoelectronics Society-SBMO Received 10 Aug., 2006; revised 2 Feb., 2007; accepted 14 May, 2007
ISSN 1516-7399

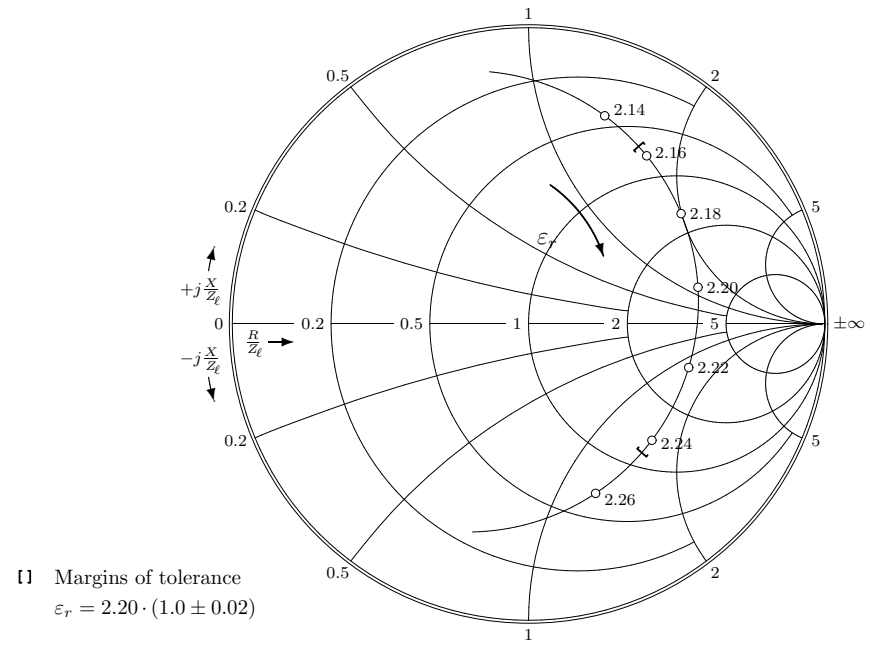

Fig. 11. Input impedance of a planar patch antenna as a function of the relative permittivity ε_r, $l_x^{\mathrm{p}} = 35\,\mathrm{mm}$, $l_y^{\mathrm{p}} = 35\,\mathrm{mm}$, $l_z^{\mathrm{c}} = 0.762\,\mathrm{mm}$, $l_x^{\mathrm{c}} = 52.5\,\mathrm{mm}$, $l_y^{\mathrm{c}} = 52.5\,\mathrm{mm}$, $l_x^{\mathrm{F}} = 17.5\,\mathrm{mm}$, $l_y^{\mathrm{F}} = 7.5\,\mathrm{mm}$, $\tan\delta = 0.0008$, $Z_\ell = 50\,\Omega$, $f = 2.79\,\mathrm{GHz}$.

to a feed network is caused by a modest alteration of curvature in practical applications, since the fluctuations of the input impedance resulting from curvature changes are not significant.

As final investigation, the influence of permittivity variations on the input impedance of a patch antenna is analysed. For this, the same antenna considered previously in Fig. 6 is used, where the substrate is characterised by $\varepsilon_r = 2.20$. The relative permittivity of a dielectric substrate material is commonly specified with a tolerance of $\pm 2\%$ to $\pm 4\%$. The input impedance of the patch element is depicted as function of the relative permittivity in Fig. 11, where the operating frequency f is kept constant at $2.79\,\mathrm{GHz}$. The Smith chart emphasizes the strong impact of permittivity variations on the input impedance and resonance frequency of a patch antenna, which shows that permittivity tolerances represent uncertainties which potentially generate deviations between computed and measured results.

V. Conclusion

A finite elements-boundary integral procedure has been developed to analyse the impedance properties and radiation characteristics of planar and curved microstrip patch antennas. The method has initially been validated by analysing the impedance characteristics of a planar patch antenna fed at different probe locations and by analysing the impact of varying probe diameters. The effect of the cavity size on the radiation and impedance characteristics has been investigated, and it has been shown that the cavity dimensions have no significant impact on the performance of a single patch antenna, as long as the cavity walls are sufficiently distant from the edges of the patch, such that the fringing fields are not perturbed. Simulations revealed that the characteristics of a single patch element are not significantly altered through a modest variation of curvature. Computed results have been shown to

Brazilian Microwave and Optoelectronics Society-SBMO Received 10 Aug., 2006; revised 2 Feb., 2007; accepted 14 May, 2007
ISSN 1516-7399

be in good agreement with measurements.

APPENDIX

The Green's function for the planar structure is given by

$$\vec{\vec{G}}(\vec{r},\vec{r}\,') = -\left(\vec{\vec{I}} + \frac{1}{k_0^2}\nabla\nabla\right)\frac{e^{-jk_0|\vec{r}-\vec{r}\,'|}}{2\pi|\vec{r}-\vec{r}\,'|} \tag{25}$$

where $\vec{\vec{I}}$ symbolizes the unit dyad. The required components of the dyadic Green's function on the surface of a cylinder with radius ρ are given by

$$\begin{aligned}
G^{\phi\phi}(\vec{r},\vec{r}\,') &= \frac{1}{(2\pi)^2}\sum_{n=-\infty}^{\infty}\int_{-\infty}^{\infty}\frac{1}{\rho k_\rho}\left[\left(\frac{nk_z}{\rho k_\rho k_0}\right)^2\frac{H_n^{(2)}(\rho k_\rho)}{H_n'^{(2)}(\rho k_\rho)} - \frac{H_n'^{(2)}(\rho k_\rho)}{H_n^{(2)}(\rho k_\rho)}\right]e^{-jk_z(z-z')}e^{-jn(\phi-\phi')}\,dk_z\,,\\
G^{\phi z}(\vec{r},\vec{r}\,') &= \frac{-1}{(2\pi)^2}\sum_{n=-\infty}^{\infty}\int_{-\infty}^{\infty}\frac{nk_z}{\rho^2 k_\rho k_0^2}\frac{H_n^{(2)}(\rho k_\rho)}{H_n'^{(2)}(\rho k_\rho)}\,e^{-jk_z(z-z')}e^{-jn(\phi-\phi')}\,dk_z\,,\\
G^{zz}(\vec{r},\vec{r}\,') &= \frac{1}{(2\pi)^2}\sum_{n=-\infty}^{\infty}\int_{-\infty}^{\infty}\frac{k_\rho}{\rho k_0^2}\frac{H_n^{(2)}(\rho k_\rho)}{H_n'^{(2)}(\rho k_\rho)}\,e^{-jk_z(z-z')}e^{-jn(\phi-\phi')}\,dk_z\,.
\end{aligned} \tag{26}$$

$H_n^{(2)}$ denotes the Hankel function of second kind and order n, and $H_n'^{(2)}$ its derivative with respect to the argument. k_ρ and k_z represent the radial and axial wavenumbers respectively. $G^{z\phi}(\vec{r},\vec{r}\,')$ is equal to $G^{\phi z}(\vec{r},\vec{r}\,')$. A detailed analysis of Green's functions is given in [33] and asymptotic solutions for the fields on the surface of a cylinder are discussed in [10], [34], [35].

REFERENCES

[1] A. Bayliss and E. Turkel, "Radiation boundary conditions for wave-like equations," *Communications on Pure and Applied Mathematics*, vol. 33, no. 6, pp. 707–725, Nov. 1980.

[2] R. Mittra, O. Ramahi, A. Khebir, R. Gordon, and A. Kouki, "A review of absorbing boundary conditions for two and three-dimensional electromagnetic scattering problems," *IEEE Transactions on Magnetics*, vol. 25, no. 4, pp. 3034–3039, July 1989.

[3] J.-P. Berenger, "A perfectly matched layer for the absorption of electromagnetic waves," *Journal of Computational Physics*, vol. 114, no. 2, pp. 185–200, Oct. 1994.

[4] Z. S. Sacks, D. M. Kingsland, R. Lee, and J.-F. Lee, "A perfectly matched anisotropic absorber for use as an absorbing boundary condition," *IEEE Transactions on Antennas and Propagation*, vol. 43, no. 12, pp. 1460–1463, Dec. 1995.

[5] O. M. Ramahi and R. Mittra, "Finite element solution for a class of unbounded geometries," *IEEE Transactions on Antennas and Propagation*, vol. 39, no. 2, pp. 244–250, Feb. 1991.

[6] J.-M. Jin, J. L. Volakis, and J. D. Collins, "A finite-element–boundary-integral method for scattering and radiation by two- and three-dimensional structures," *IEEE Antennas and Propagation Magazine*, vol. 33, no. 3, pp. 22–32, June 1991.

[7] J. Gong, J. L. Volakis, A. C. Woo, and H. T. G. Wang, "A hybrid finite element-boundary integral method for the analysis of cavity-backed antennas of arbitrary shape," *IEEE Transactions on Antennas and Propagation*, vol. 42, no. 9, pp. 1233–1242, Sept. 1994.

[8] J.-M. Jin and J. L. Volakis, "A hybrid finite element method for scattering and radiation by microstrip patch antennas and arrays residing in a cavity," *IEEE Transactions on Antennas and Propagation*, vol. 39, no. 11, pp. 1598–1604, Nov. 1991.

[9] ——, "Scattering and radiation analysis of three-dimensional cavity arrays via a hybrid finite-element method," vol. 41, no. 11, pp. 1580–1586, Nov. 1993.

[10] L. C. Kempel and J. L. Volakis, "Scattering by cavity-backed antennas on a circular cylinder," *IEEE Transactions on Antennas and Propagation*, vol. 42, no. 9, pp. 1268–1279, Sept. 1994.

Brazilian Microwave and Optoelectronics Society-SBMO Received 10 Aug., 2006; revised 2 Feb., 2007; accepted 14 May, 2007
ISSN 1516-7399

[11] A. D. Brown, J. L. Volakis, L. C. Kempel, and Y. Y. Botros, "Patch antennas on ferromagnetic substrates," *IEEE Transactions on Antennas and Propagation*, vol. 47, no. 1, pp. 26–32, Jan. 1999.
[12] P. Soudais, H. Stève, and F. Dubois, "Scattering from several test-objects computed by 3-D hybrid IE/PDE methods," *IEEE Transactions on Antennas and Propagation*, vol. 47, no. 4, pp. 646–653, Apr. 1999.
[13] J. L. Volakis, A. Chatterjee, and J. Gong, "A class of hybrid finite element methods for electromagnetics: A Review," *Journal of Electromagnetic Waves and Applications*, vol. 8, no. 9/10, pp. 1095–1124, Sept. 1994.
[14] J. L. Volakis, T. Özdemir, and J. Gong, "Hybrid finite-element methodologies for antennas and scattering," *IEEE Transactions on Antennas and Propagation*, vol. 45, no. 3, pp. 493–507, Mar. 1997.
[15] J. Jin, *The Finite Element Method in Electromagnetics*. New York: John Wiley & Sons, Inc., 1993.
[16] J. L. Volakis, A. Chatterjee, and L. C. Kempel, *Finite Element Method for Electromagnetics*, ser. IEEE Press Series on Electromagnetic Wave Theory. New York: IEEE Press, 1998.
[17] P. P. Silvester and R. L. Ferrari, *Finite Elements for Electrical Engineers*, 2nd ed. Cambridge: Cambridge University Press, 1990.
[18] A. Kost, *Numerische Methoden in der Berechnung elektromagnetischer Felder*. Berlin, Heidelberg, New York: Springer-Verlag, 1994.
[19] W. Sun and C. A. Balanis, "Edge-based FEM solution of scattering from inhomogeneous and anisotropic objects," *IEEE Transactions on Antennas and Propagation*, vol. 42, no. 5, pp. 627–632, May 1994.
[20] A. J. Sangster and R. T. Jacobs, "Mutual coupling in conformal microstrip patch antenna arrays," *IEE Proceedings on Microwaves, Antennas and Propagation*, vol. 150, no. 4, pp. 191–196, Aug. 2003.
[21] R. F. Harrington, *Field Computation by Moment Methods*. New York: IEEE Press, 1993.
[22] C.-T. Tai, *Generalized Vector and Dyadic Analysis*. New York: IEEE Press, 1991.
[23] R. E. Collin, *Field Theory of Guided Waves*, 2nd ed. New York: IEEE Press, 1991.
[24] W. C. Chew, *Waves and Fields in Inhomogeneous Media*, ser. IEEE Press Series on Electromagnetic Waves. New York: IEEE Press, 1995.
[25] Y. Saad, *Iterative Methods for Sparse Linear Systems*. Boston: PWS Publishing Company, 1996.
[26] T. K. Sarkar, "On the application of the generalized biconjugate gradient method," *Journal of Electromagnetic Waves and Applications*, vol. 1, no. 3, pp. 223–242, Mar. 1987.
[27] D. M. Pozar, "Input impedance and mutual coupling of rectangular microstrip antennas," *IEEE Transactions on Antennas and Propagation*, vol. 30, no. 6, pp. 1191–1196, Nov. 1982.
[28] T. J. Peters and J. L. Volakis, "Application of a conjugate gradient FFT method to scattering from thin planar material plates," *IEEE Transactions on Antennas and Propagation*, vol. 36, no. 4, pp. 518–526, Apr. 1988.
[29] J.-M. Jin and J. L. Volakis, "A biconjugate gradient FFT solution for scattering by planar plates," *Electromagnetics*, vol. 12, pp. 105–119, Dec. 1992.
[30] C. Van Loan, *Computational Frameworks for the Fast Fourier Transform*. Philadelphia, PA: SIAM Publications, 1992.
[31] T. K. Sarkar, Ed., *Progress in Electromagnetic Research, Pier 5: Application of Conjugate Gradient Method to Electromagnetics and Signal Analysis*. New York, Amsterdam, London: Elsevier, 1990.
[32] E. V. Sohtell, "Microstrip antennas on a cylindrical surface," in *Handbook of Microstrip Antennas, Vol. 2*, ser. IEE Electromagnetic Waves Series, J. R. James and P. S. Hall, Eds. London: Peter Peregrinus Ltd., 1989, ch. 22, pp. 1227–1256.
[33] C.-T. Tai, *Dyadic Green Functions in Electromagnetic Theory*, 2nd ed., ser. IEEE Press Series on Electromagnetic Waves. New York: IEEE Press, 1994.
[34] T. S. Bird, "Comparison of asymptotic solutions for the surface field excited by a magnetic diplole on a cylinder," *IEEE Transactions on Antennas and Propagation*, vol. 32, no. 11, pp. 1237–1244, Nov. 1984.
[35] P. H. Pathak and N. Wang, "Ray analysis of mutual coupling between antennas on a convex surface," *IEEE Transactions on Antennas and Propagation*, vol. 29, no. 6, pp. 911–922, Nov. 1981.

Brazilian Microwave and Optoelectronics Society-SBMO Received 10 Aug., 2006; revised 2 Feb., 2007; accepted 14 May, 2007
ISSN 1516-7399